Parametric Study for Calculating Surface Deflection Using the Method of Images

IOP Conf. Series: Materials Science and Engineering **576** (2019) 012037 doi:10.1088/1757-899X/576/1/012037

Parametric Study for Calculating Surface Deflection Using the Method of Images

Y An[1], R Zhang[1], P Li[1], D Luo[1], and X Jin[1,2]

[1]State Key laboratory of Mechanical Transmissions, Chongqing University, Chongqing 400030, China
[2]College of Aerospace Engineering, Chongqing University, Chongqing, 400030, China

Corresponding Author's E-mail: jinxq@cqu.edu.cn

Abstract. The solution of the elastic field for inclusions in an elastic half space has been applied widely in many contact analyses and engineering designs. A popular method to solve the half-space inclusion problem resorts to the method of images, where the solution is decomposed into 3 components consisting of the full space inclusion, mirrored inclusion, and the surface traction cancellation. In the process of cancelling the redundant surface tractions determined from a full space inclusion problem, the computation domain is supposed to be limited in a finite size and there is inevitably truncation error. It has not been quantitatively investigated how the truncation error will influence the accuracy of the numerical computations based on the method of images. This work studies the deflection of the boundary surface of a half-space containing an Eshelby inclusion. Errors due to mesh refinement and domain truncation are quantitatively analyzed. Parametric studies are performed for a systematic examination of surface redundant tractions and their influences.

1. Introduction

The inclusion problem provides a unified treatment for a variety of subjects and has been regarded as being of fundamental importance to many research branches in material science. The solutions for the half-space inclusions usually tend to be more intricate and complex, and the derivation for this problem may be laborious and time-consuming. The general problem of arbitrarily shaped inclusion in half space usually solved by the method of images which is straightforward and effective.

Eshelby [1] first solved the problem of the interior elastic field of an ellipsoidal inclusion subjected to uniform eigenstrain in an infinite space in 1957. However, the exterior elastic field is much more complicated. The explicit complete solutions of an ellipsoidal inclusion in full space was analytically proposed by Jin et al [2]. Chiu [3] solved the displacement gradient due to cuboidal inclusion with uniform eigenstrains in a full elastic space, and further [4] proposed a strategy for solving the inclusion in a semi-infinite space via the method of images. In practical engineering design, the inclusions might be any arbitrary shape and distributed in a random manner. Zhou et al. [5] proposed a fast numerical method to solve 3D arbitrarily shaped inclusions in half-space. Liu et al [6] derived a set of explicit formulas in terms of the Galerkin vectors for the displacements and stresses in half space and ingeniously proposed the Fast Fourier Transform (FFT) techniques combining convolution and correlations for numerical computations of the half-space inclusion problem. Their half-space solutions to the cuboidal inclusion subjected in uniform eigenstrains are exact and represented in closed-form, and therefore could be used as the elementary solution for solving arbitrarily shaped

inclusion by breaking up the inclusion domain into multiple cuboids. Further, Zhou et al [7] proposed a mesh differential refinement scheme for solving elastic fields of half-space inclusion problems.

This paper intends to examine the numerical error issues in determining the surface deflection caused by distribution of eigenstrains (or inclusion) in a half space using the method of images [4]. The method of images is often adopted for solving a half-space inclusion problem, which is constructed by cancelling the redundant surface tractions determined from a full space inclusion problem. However, truncation errors would inevitably appear in the numerical implementation, particularly when an inclusion is located close to the surface of the half space. Several benchmark examples are provided to demonstrate the effects on the surface displacement for a variety of relevant parameters.

2. Formulation

2.1. Method of images

Consider an isotropic and homogeneous arbitrarily shaped inclusion embedded in an elastic semi-infinite space which is defined by $x_3 \geq 0$ Chiu [4] proposed that, the solution of inclusion in a semi-infinite space may be obtained by utilizing the method of images. According to the superposition principle, an isotropic inclusion in a semi-infinite space may be decomposed into three components (figure 1): (1) and (2) are the original and the mirror inclusions with specified eigenstrains in the full space respectively, and (3) is the solution of normal stress distributed on the free surface of semi-infinite space.

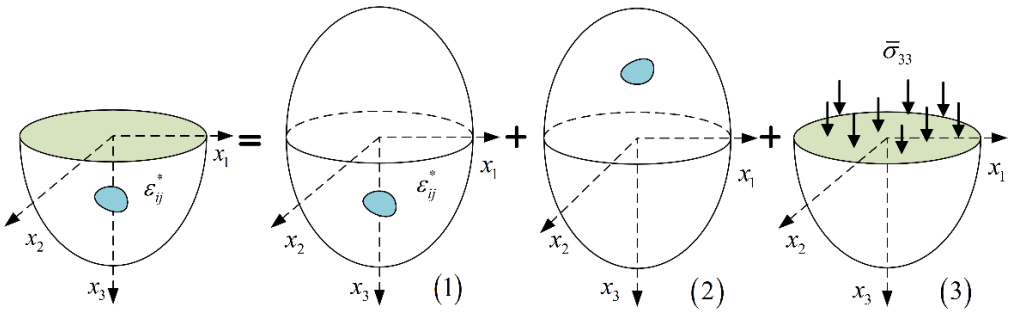

Figure 1. Decomposition of the half-space solution into three components.

By the Voigt notation [8], the prescribed eigenstrain uniformly distributed in the inclusion of domain (1) may be written as

$$\varepsilon_{ij}^* = \left[\varepsilon_{11}^*,\ \varepsilon_{22}^*,\ \varepsilon_{33}^*,\ 2\varepsilon_{23}^*,\ 2\varepsilon_{13}^*,\ 2\varepsilon_{12}^*\right]^T \tag{1}$$

The resulting displacement at an arbitrary field point in the inclusion of domain (1) may be represented in a matrix form as follows

$$\begin{bmatrix} u_1 \\ u_2 \\ u_3 \end{bmatrix} = \begin{bmatrix} w_{111} & w_{122} & w_{133} & w_{123} & w_{113} & w_{112} \\ w_{211} & w_{222} & w_{233} & w_{223} & w_{213} & w_{212} \\ w_{311} & w_{322} & w_{333} & w_{323} & w_{313} & w_{312} \end{bmatrix} \begin{bmatrix} \varepsilon_{11}^* \\ \varepsilon_{22}^* \\ \varepsilon_{33}^* \\ 2\varepsilon_{23}^* \\ 2\varepsilon_{13}^* \\ 2\varepsilon_{12}^* \end{bmatrix} \tag{2}$$

where w_{ijk} denote the influence coefficients of the original inclusion in full space. Moreover, the symmetric inclusion of domain (2) is subjected to a mirror eigenstrainIt is worthwhile to note that the eigenstrain

$$\varepsilon_{ij}'^{*}=\left[\varepsilon_{11}^{*},\ \varepsilon_{22}^{*},\ \varepsilon_{33}^{*},\ -2\varepsilon_{23}^{*},\ -2\varepsilon_{13}^{*},\ 2\varepsilon_{12}^{*}\right]^{T} \tag{3}$$

After the summation of the first two solutions, the normal stress on the symmetry plane $x_3=0$ is twice and the symmetry plane is free of shear tractions. Besides, the normal displacement along the surface cancels. According to the method of Images [4], the traction-free condition at the boundary surface is obtained by superimposing the solution for a half space under normal plane stress σ_{33} which is opposite to the resultant stresses after superposing problems (1) and (2) in figure 1.

In view of the superposition of three components, the displacement of an arbitrary shaped inclusion in half space may be expressed as

$$u_i(\mathbf{x})=\int_{\Omega_1} w_{ikl}^{(1)}(\mathbf{x}-\mathbf{x}')\varepsilon_{kl}^{*}d\Omega_1+\int_{\Omega_2} w_{ikl}^{(2)}(\mathbf{x}-\mathbf{x}')\varepsilon_{kl}'^{*}d\Omega_2+\sum\sum\chi_{i3}(\mathbf{x}-\mathbf{x}')p_{30} \tag{4}$$

where $\chi_{i3}(\mathbf{x}-\mathbf{x}')$ is the response function, also termed as the influence coefficient [8], of elemental normal contact force uniformly distributed on the rectangular patch, and p_{30} is a normal stress whose magnitude is evaluated at the centre of the rectangle.

2.2. Love's rectangular contact solution

In abovementioned equation, Solutions (1) and (2) (figure 1) have been determined in closed-form, whose details can be found in [6]. The solution (3) is solved numerically by discretizing the computational domain into a number of rectangular patches at the symmetry plane. The elastic field produced by a uniform rectangular patch loading is solved by employing Love's rectangular contact solution, which has been comprehensively discussed and recorded by an effective notation in conjunction with the FFT algorithm [9].

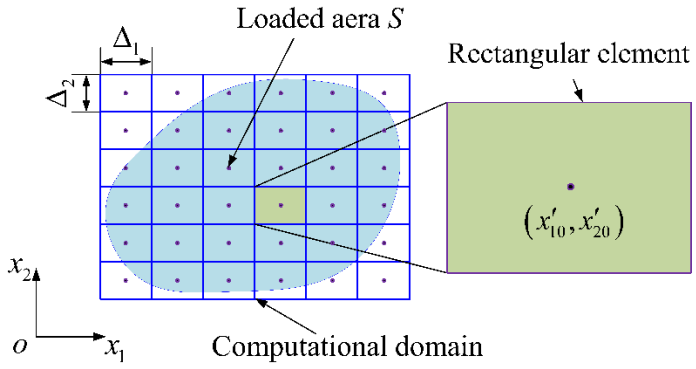

Figure 2. Discretization of the computation domain using a uniform rectangular mesh.

Consider a loaded area S of the symmetry surface as a computational domain which is discretized by $N_1\times N_2$ uniform rectangular meshes with each sides of length Δ_1 and Δ_2 (figure 2). Each grid point labelled by [*i*, *j*] is placed at the centre of the elements and assumed to be subjected uniform stress whose magnitude is evaluated at the centre of the rectangle. The indices *i* and *j* refer to the columns and rows of each grid, respectively. All of the grid points are denoted by I_g

$$I_g=\{[i,j]:\ 1\le i\le N_1,\ 1\le j\le N_2\} \tag{5}$$

The surface displacement of single element could be written in matrix form as follows

$$\begin{bmatrix} u_1 \\ u_2 \\ u_3 \end{bmatrix} = \begin{bmatrix} \chi_{11} & \chi_{12} & \chi_{13} \\ \chi_{21} & \chi_{22} & \chi_{23} \\ \chi_{31} & \chi_{32} & \chi_{33} \end{bmatrix} \begin{bmatrix} p_{10} \\ p_{20} \\ p_{30} \end{bmatrix} \tag{6}$$

where p_{j0}, $(j=1,2,3)$ is the magnitude of the uniform stress acting on the centre of the rectangle along the x_j axis; and χ_{ij} is termed as the elementary influence coefficient which relate the stress to the surface displacement at the surface point.

The computational domain in problem (3) (cf. figure 1) is numerically discretized by rectangular patches, each of which is assumed to be subjected uniform normal stress p_{30} .The surface displacement could be solved by superposing contributions of each element. For example, the surface deflection at grid point [i, j] may be written as

$$\bar{u}_3^{[i,j]} = \sum_{k=1}^{N_1} \sum_{l=1}^{N_2} \chi_{33}^{i-k,j-l} p_{30}^{[k,l]}, \quad [i,j] \in I_g \tag{7}$$

As a result, the solution (3) can be solved by discretizing the computational domain into a number of rectangular patches and superposing contributions of each element.

3. Results and discussions

A benchmark example of a cuboidal inclusion is given in this section to explore the effects on the surface redundant traction and the surface displacement for different depth, shape and meshes. The related parameters for the baseline case in the computation are listed in table 1. The different results can be compared to each other by considering that the parameters for the baseline case are common between all examples of simulations.

Table 1. Parameters of matrix and the cuboidal inclusion for the baseline case.

Parameters	Values
Young's modulus, E (GPa)	210
Poisson's ratio, ν	0.3
Eigenstrain components	$\left[\varepsilon^*\right]=10^{-3}\times\left[1\ 1\ 1\ 0\ 0\ 0\right]^T$
side length	$a=1,\ b=1,\ c=1$
Distance to the Surface	$s=1$

The variation of relative surface redundant traction and surface displacement are calculated along the x_1 axis for different depth in dimensionless form, as depicted in figures. 3 and 4 respectively. It clearly shows that the effect of the inclusion on the stress field is decreasing when the cube is located deeper below the surface. It can be noted that when the cube is located at $s=2a$, the stress field tends to be uniform and the redundant traction and the displacement on the surface is not distinct. This means that once the inclusion is far away from the surface, the value of its depth play a negligible role in determining the redundant surface traction and surface deflection. Moreover, when the value of s/a is close to zero, the redundant traction on the surface above the cube is almost a constant except at the boundary edges.

The comparison of the surface redundant traction and the surface displacement along the x_1 axis for different value of b/a and c/a is shown in figures. 5 and 6 respectively. It can be observed that

both the redundant traction and the displacement on the surface are reduced with the decreasing of the cuboidal size. Moreover, comparing the figures of the surface displacement for different shapes, it can be concluded that the effect of c on the surface displacement is concentrated inside, and the influence of b is scattered.

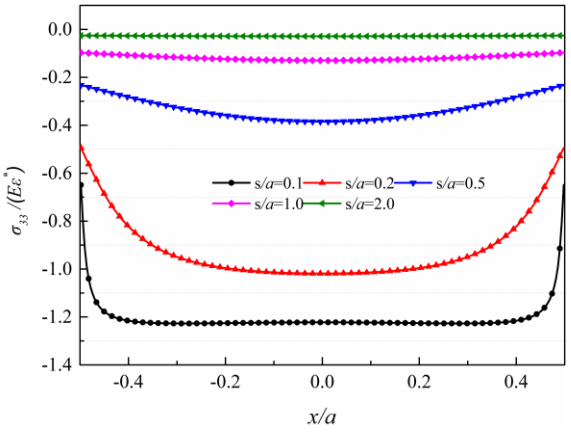

Figure 3. Variation of dimensionless surface redundant traction along the x_1 axis for different depth.

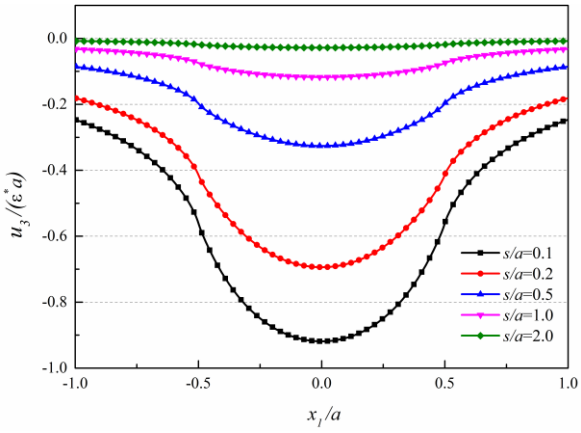

Figure 4. Variation of dimensionless surface displacement along the x_1 axis for different depth.

In the computation, the domain is discretized into 251×251 grids for the baseline case. Next, the computational domain is magnified in order to investigate the effects of the size of the computational domain. The variation of relative dimensionless surface displacement along the x_1 axis with different value of magnification $NFCTX$ is shown in figure 7. It should be noted that the resulting displacement show noticeable discrepancy from the exact solution without magnifying the size of the computational domain, but it tends to agree with the exact solution with magnification $NFCTX=3$. Further increase of the magnification factor $NFCTX$ would distinctly the occupied more computational time but shows no distinct influence (figure 7). Accordingly, there is no necessary to further enlarge the magnification factor. Therefore, in order to improve the accuracy of calculation, the size of the computational domain must be extended to some degree.

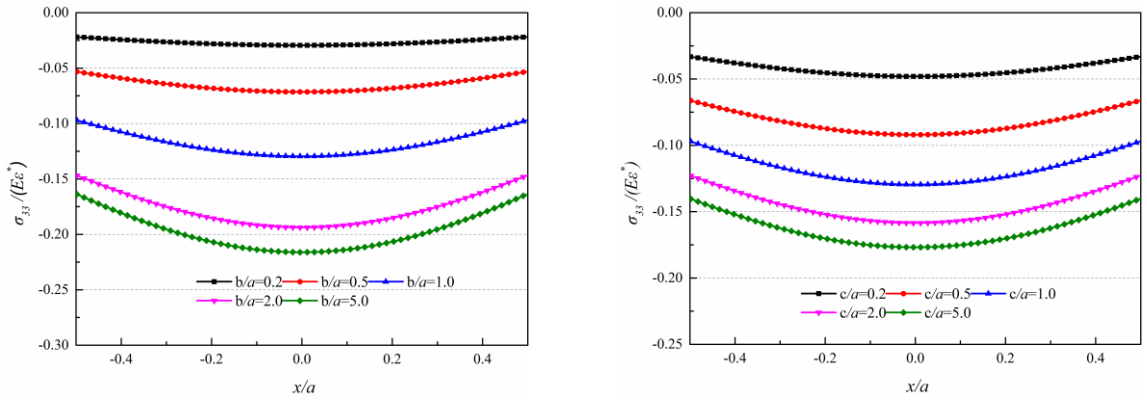

(a) (b)

Figure 5. Comparison of dimensionless surface redundant traction along the x_1 axis for different shapes: (a) b/a change; (b) c/a change.

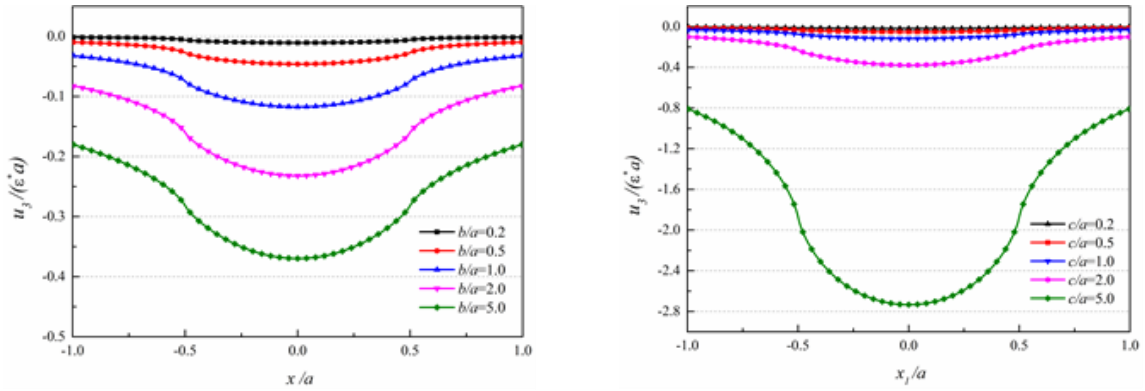

(a) (b)

Figure 6. Comparison of dimensionless surface displacement along the x_1 axis for different shapes: (a) b/a change; (b) c/a change.

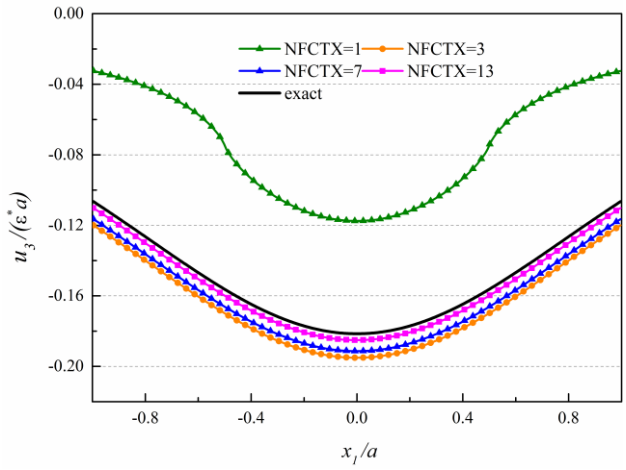

Figure 7. Variation of dimensionless surface displacement along the x_1 axis for different meshes.

4. Conclusions

The elastic field of an inclusion in a half space with eigenstrain is often complex and intricate because of the mathematical difficulties arisen from the effect of the free surface. Notwithstanding, the current work demonstrates that the stress field of an arbitrarily shaped inclusion in a half space can be solved by the method of images. The Voigt notation and the Eshelby tensor were utilized for simplifying the numerical computation and computer programming. A number of interesting parametric studies are provided in this paper in order to explore their effects on the surface displacement. It is shown that the surface displacement of the inclusion is much closer to the exact solution by magnifying the size of the computational domain. Numerical computations for half-space problems always require a large computational domain to guarantee its accuracy.

References

[1] Eshelby J D, P. Roy. Soc. Lond. Ser. A, **241** (1226), 376-396(1957)
[2] Jin X, Lyu D, Zhang X, Zhou Q, Wang Q, Keer L M, ASME. J. Appl. Mech, **83**(12), 121010-121010-12(2016)
[3] Chiu Y P, ASME. J. Appl. Mech, **44**(4), 587-590 (1977)
[4] Chiu Y P, ASME. J. Appl. Mech, **45**(2), 302-306 (1978)
[5] Zhou K, Chen W, Keer L M, Wang Q, Comput Methods Appl Math, **198**(9-12), 885-892(2009)

[6] Liu S, Jin X, Wang Z, Keer L M, Wang Q, Int. J. Plasticity, **35**(Supplement C), 135-154 (2012)
[7] Zhou Q, Jin X, Wang Z, Yang Y, Wang J, Keer L M, Wang Q, Tribol. Int, **93**, 124-136(2016)
[8] Mura T, Micromechanics of defects in solids. 2nd ed. (Springer, Dordrecht, The Netherlands, 1987)
[9] Jin X, Niu F, Zhang X, Zhou Q, Lyu D, Keer L M, Hu Y, Tribol. Int, **103**, 331-342(2016)

Acknowledgments
This work is supported by Fundamental Research Funds for the Central Universities (2018CDYJSY0055 and Nos.106112017CDJQJ328839). The authors are grateful to the Graduate Research and Innovation Foundation of Chongqing, China (Grant Nos. CYB18020 and CYB17025). X.J. would also like to acknowledge the support from the National Natural Science Foundation of China (Grant Nos. 51475057 and 51875059), and the State Key Laboratory of Mechanical Transmissions through funding (SKLMT-ZZKT-2017M15).